CHALMERS

CFD-simulations of urea-SNCR for NO_x-reduction in flue gases from biomass combustion

Master's thesis in Sustainable Energy Systems

NING GUO

Department of Applied Mechanics
CHALMERS UNIVERSITY OF TECHNOLOGY
Göteborg, Sweden 2015

MASTER'S THESIS IN SUSTAINABLE ENERGY SYSTEMS

CFD-simulations of urea-SNCR for NO_x-reduction in flue gases from biomass combustion

NING GUO

Department of Applied Mechanics
Division of Fluid Dynamics
CHALMERS UNIVERSITY OF TECHNOLOGY

Göteborg, Sweden 2015

CFD-simulations of urea-SNCR for NO_x-reduction in flue gases from biomass combustion
NING GUO

© NING GUO, 2015

Master's thesis 2015:42
ISSN 1652-8557
Department of Applied Mechanics
Division of Fluid Dynamics
Chalmers University of Technology
SE-412 96 Göteborg
Sweden
Telephone: +46 (0)31-772 1000

Chalmers Reproservice
Göteborg, Sweden 2015

CFD-simulations of urea-SNCR for NO_x-reduction in flue gases from biomass combustion
Master's thesis in Sustainable Energy Systems
NING GUO
Department of Applied Mechanics
Division of Fluid Dynamics
Chalmers University of Technology

ABSTRACT

Urea-SNCR is a technology that can reduce NO_x emissions from biomass combustion. In order to have good results of NO_x reduction in a certain urea-SNCR system, simulations are advised to be conducted, it can be used to optimize the system design, which also significantly reduces the time and costs of experimental optimization in the real plant

In the simulation, urea evaporation and decomposition and NO_x reduction are two important processes that needs to be simulated. In this thesis work, a CFD model ($k - \epsilon$ model, chemical-turbulence interaction model and discrete random walk model) is used to simulate the urea evaporation and decomposition. A CSTR (Continuous Stirred-Tank Reactor) model, a PFR (Plugged Flow Reactor) model and the CFD model are all evaluated in simulations of the NO_x reduction process.

The CSTR, PFR, and CFD models are tested at different conditions (temperature, geometry, retention time, injection points, etc.) for a complete urea-SNCR process. Under the given conditions, the effects of turbulent velocity fluctuations on the urea spray, the effects of mixing and chemical kinetics on each reaction, the effects of temperature and retention time on the NO_x reduction and the reaction selectivities are studied. Then the CFD model is validated against experimental data from a power plant in Rörvik, which shows the CFD model is suitable for the simulation. Based on the CFD simulations, a new injection strategy for urea-water mixture is evaluated.

Keywords: urea-SNCR, CSTR, PFR, CFD

ACKNOWLEDGEMENTS

I would like to express my gratitude for finishing my master's thesis.

Firstly, I greatly thank my supervisor Assistant Professor Henrik Ström for his great knowledge, guidance and patience. Without him, this work could not reach the level it is now.

I would also like to give credits to Oskar Finnermann for his contribution in CSTR, PFR and CFD simulations and report proof reading. Narges Razmjoo, Michael Strand and Jan Brandin from Linnaeus University provided experimental data and insightful input, which is appreciated.

Professor Srdjan Sasic is kind enough to act as my examiner. Special thanks to everyone at the Division of Fluid Dynamics at Chalmers for a friendly working environment and nice coffee breaks.

This master thesis is partly funded by Chalmers Avencez Scholarship.

CONTENTS

Abstract i

Acknowledgements i

Contents iii

1 Introduction 1

2 Theory 2

2.1 Urea SNCR process 2

2.1.1 Urea evaporation and decomposition 2

2.1.2 NO_x reduction 3

2.2 Simulation models 3

2.2.1 CSTR model 3

2.2.2 PFR model 4

2.2.3 CFD model 4

2.2.4 Chemical-turbulence interaction model 5

2.2.5 Euler-Lagrange model and discrete random walk model 6

3 Case specifications 8

3.1 Urea evaporation and decomposition 8

3.2 NO_x reduction 9

3.3 Whole process 10

3.3.1 Simple pipe 11

3.3.2 Rörvik plant 11

4 Results and discussions 13

4.1 Effects of discrete random walk model on urea spray injection simulation 13

4.2 Effects of mixing and chemical kinetics on each reaction 14

4.3 Effects of temperature and retention time on NO_x reduction 14

4.4 Model selection 15

4.5 CFD model validation 16

4.6 New injection test 17

5 Conclusions 19

6 Future work 20

References 21

I Appended Paper A 25

1 Introduction

One way to reduce CO_2 emissions from the energy production industry is to produce sustainable energy by using biomass combustion boilers. However, part of the nitrogen in the biomass fuel and air is converted to nitrogen oxides (NO_x), which is harmful to the environment and public health [1]. To solve this problem, one possibility is to use urea to react with the exhaust gases from combustion so that NO_x can be converted to nitrogen (N_2). In other words, ammonia (NH_3) can be produced from urea decomposition and then reduce NO_x to N_2. Urea-SNCR (selective non-catalytic reduction) technology is one feasible way to do it.

In the industries, in order to save time and money, simulations are often conducted before experiments are carried out. Numerical simulations, when carefully executed, have the potential to reduce the time from prototype to final solution by orders of magnitude. In these cases, model selections are crucial. A simplified model is computationally cheap, but may be far away for the reality. A complicated model is close to the real practice but maybe too computationally expensive.

The Urea-SNCR process can be divided into two parts (sub-processes): 1) urea evaporation and decomposition, in which urea-water mixture is injected to the flue gases from biomass combustion, decomposes and produces NH_3; 2) NO_x reduction, in which NH_3 reduces NO into N_2. Different models must be chosen to simulate each aspect of each sub-process. Different combinations of models affect the simulation results and the computational resources required.

In this master thesis, a Continuous Stirred-Tank Reactor (CSTR) model, a Plug Flow Reactor (PFR) model and a Computational Fluid Dynamics (CFD) model are used to simulate the urea-SNCR process. Comparing with experimental data from a Rörvik power plant, a guideline of model selection has been proposed. A new injection strategy for this power plant is also tested in the simulation.

Besides model selection, the impact of turbulent velocity fluctuations on the convective heat transfer urea droplets is also studied.

However, the biomass combustion process before the urea-SNCR system will not be studied in this thesis.

2 Theory

In this chapter, the theoretical background of the urea SNCR process and the models that are used to simulate this process are explained.

2.1 Urea SNCR process

The urea SNCR process can be divided into two parts: 1) urea evaporation and decomposition, and 2) NO_x reduction.

2.1.1 Urea evaporation and decomposition

First of all, urea-water mixture droplets, whose temperature is relatively low, are injected into biomass combustion flue gases, whose temperature is relatively high. Due to the temperature difference, urea-water particles are heated and vaporize to water vapor and urea vapor. The evaporation process can therefore be modeled as two parallel evaporation fluxes.

In the CFD simulations, the convection/diffusion controlled model is used for mass transportation [2][3]:

$$\frac{\mathrm{d}m_i}{\mathrm{d}t} = A_p k_{c,i} \rho_\infty \ln\left(1 + B_{i,m}\right) \tag{2.1}$$

where m is the mass, t is the time, k_c is the mass transfer coefficient, A_p is the droplet surface area, ρ_∞ is the density of bulk gas, M_w is the molecular weight, B_m is the Spalding mass number and subscript i denotes the species component i.

The heat balance is defined as

$$m_p C_p \frac{\mathrm{d}T_p}{\mathrm{d}t} = hA_p\left(T_\infty - T_p\right) + \sum_i \frac{\mathrm{d}m_i}{\mathrm{d}t}\left(h_{vap,i}\right) \tag{2.2}$$

where C_p is the heat capacity of the particle, T_p is the particle temperature, h is the heat transfer coefficient for the convective/diffusion controlled model, T_∞ is the local temperature of continuous phase, $\frac{\mathrm{d}m_i}{\mathrm{d}t}$ is from Eq. (2.1), h_{vap} is the latent heat of vaporization.

According the work of Lundström et al. [4], the relationship of urea vapor pressure, p_{urea} [Pa], and temperature, T [K] (within the range of 406K-550K) is simulated as in (2.3):

$$\log_{10} p_{urea}(T) = A - \frac{B}{C+T} \tag{2.3}$$

where A, B and C are constants as stated in Table 2.1.

Constant	A	B	C
Value	1.1663E+01	4.0854E+03	3.3953E-3

Table 2.1: Antoine constants for urea vapor pressure and temperature (406K-550K)

In this work, the water vapor pressure is modelled using piecewise-linear method as in Table 2.2 according to the Fluent database.

Temperature	Pressure	Temperature	Pressure	Temperature	Pressure	Temperature	Pressure
273	610	274	657	275	706	280	1002
284	1329	290	1937	295	2658	300	3565
307	5316	310	6275	315	7974	320	10612
325	13289	330	17308	340	26579	350	41877
356	53158	360	62498	370	90935	371	94295
372	97757	373	101000				

Table 2.2: Saturation pressure [Pa] and temperature [K] of water vapor

Then the urea vapor starts to break down, as seen in Reaction {2.1} and {2.2}, these chemical reactions are chosen based on the work of Østberg et al. [5]. The reaction rate parameters are listed in Table 2.3.

$$\mathrm{CO(NH_2)_2} \rightarrow \mathrm{NH_3} + \mathrm{HNCO} \tag*{\{2.1\}}$$

$$\mathrm{CO(NH_2)_2} + \mathrm{H_2O} \rightarrow 2\mathrm{NH_3} + \mathrm{CO_2} \tag*{\{2.2\}}$$

In Table 2.3, A is the pre-exponent factor in m-mol-s, b is the temperature exponent and E is the activation energy in J/mol.

Reaction	A	b	E
{2.1}	1.27E+04	0	65048.109
{2.2}	6.13E+04	0	87819.133

Table 2.3: Simplified chemical process of urea breakdown

In Reaction {2.1}, only half of the N in $\mathrm{CO(NH_2)_2}$ is converted to $\mathrm{NH_3}$ while all of the N in $\mathrm{CO(NH_2)_2}$ is converted to $\mathrm{NH_3}$ in Reaction {2.2}.

2.1.2 $\mathrm{NO_x}$ reduction

In the NO_x reduction process, $\mathrm{NH_3}$, produced in the urea breakdown, can reduce NO, produced from biomass combustion, to $\mathrm{N_2}$. But $\mathrm{NH_3}$ can also be oxidized by $\mathrm{O_2}$ into NO. As seen in Reaction {2.3}, {2.4} and Table 2.4, the reaction rates are calculated based on the work of Rota et al. [6]. The variables and units in Table 2.4 and 2.3 are consistent.

$$\mathrm{NO} + \mathrm{NH_3} + 1/4\mathrm{O_2} \rightarrow \mathrm{N_2} + 3/2\mathrm{H_2O} \tag*{\{2.3\}}$$

$$\mathrm{NH_3} + 5/4\mathrm{O_2} \rightarrow \mathrm{NO} + 3/2\mathrm{H_2O} \tag*{\{2.4\}}$$

Reaction	A	b	E
{2.3}	4.24E+02	5.30	349937.06
{2.4}	3.50E-01	7.65	524487.005

Table 2.4: Simplified chemical process of NOx reduction

2.2 Simulation models

There are several different reactor models that are used industrially to simulate the urea SNCR process. These models are based on different assumptions regarding the flow field (and thus the mixing) in the urea SNCR system. In this work, these different models are considered: the CSTR model, the PFR model and a full CFD set up.

2.2.1 CSTR model

According to Roberts et al. [7], the ideal Continuous Stirred-Tank Reactor (CSTR) model is characterized by perfect mixing, which means it assumes that the temperature and concentration are uniform in the reactor.

The conservation equation of mass for a given species in a CSTR reads:

$$\frac{\mathrm{d}\rho Y_i V}{\mathrm{d}t} = [uA\rho Y_i]_{in} - [uA\rho Y_i]_{out} - \dot{r}_i \tag{2.4}$$

where ρ is density, Y is mass fraction, V is volume, t is time, u is velocity, A is the cross-sectional area, r is the net reaction rate and subscript i means different species, *in* and *out* represent the inlet and the outlet respectively. Each term in Eq. (2.4) is accumulation term, incoming convective term, outgoing convective term and source term respectively.

Since N_2 makes up the majority of the flue gases and the molar differences between reactants and products in Reaction {2.3} and {2.4} is not large, it is assumed equimolarity in the CSTR model in this thesis work, which reduces Eq. (2.4) into

$$V\frac{\mathrm{d}C_i}{\mathrm{d}t} = uA\left(C_{i,in} - C_i\right) - r_i \tag{2.5}$$

where C is the molar concentration. Since the average residence time is

$$\tau = \frac{V}{uA} \tag{2.6}$$

Eq. (2.5) now is converted to

$$\frac{\mathrm{d}C_i}{\mathrm{d}t} = \frac{C_{i,in} - C_i}{\tau} - r_i \tag{2.7}$$

It is assumed to be steady state, so

$$0 = \frac{C_{i,in} - C_i}{\tau} - r_i \tag{2.8}$$

Eq. (2.8) is the base of the Matlab simulation of CSTR model.

2.2.2 PFR model

In a plug flow reactor (PFR) model [7], the most common one-dimensional reactor model, it is often assumed that:

1. In the axial direction (flow direction), there is no mixing (no diffusion);
2. The properties in the flow perpendicular direction are uniform;

In this thesis work, it is also assumed that:

1. The temperature is constant;
2. The state is steady;
3. The ideal gas law applies.

The differential conservation of species for a PFR reads

$$\rho\frac{\partial Y_i}{\partial t} = -\rho\frac{\partial\left(uY_i\right)}{\partial x} + m''' \tag{2.9}$$

where the terms represent an accumulation term, a convective transportation term and a source term respectively.

Since it is steady state Eq. (2.9) is converted into

$$\rho\frac{\partial\left(uY_i\right)}{\partial x} = m''' \tag{2.10}$$

Similar to the CSTR model, assuming equimolarity, Eq. (2.10) can be rewritten to

$$u\frac{\mathrm{d}C_i}{\mathrm{d}x} = r_i \tag{2.11}$$

and this is base of the Matlab simulation of PFR model.

2.2.3 CFD model

For incompressible flow the continuity equation reads [8]

$$\frac{\partial U_j}{\partial x_j} = 0 \tag{2.12}$$

and the Navier-Stokes equation reads [8]

$$\frac{\partial U_i}{\partial t} + U_j\frac{\partial U_i}{\partial x_j} = -\frac{1}{\rho}\frac{\partial P}{\partial x_i} + \nu\frac{\partial^2 U_i}{\partial x_j \partial x_j} \tag{2.13}$$

In Reynolds decomposition [9], an instantaneous variable can be divided into a mean part and a fluctuating part. Take velocity as an example:

$$\vec{U} = \overline{\vec{U}} + u \tag{2.14}$$

Instantaneous velocity = Mean velocity + Fluctuating velocity

therefore, the Eq. (2.12) can be rewritten as

$$\frac{\partial \overline{U_i}}{\partial x_i} = 0 \tag{2.15}$$

and (2.13) can be rewritten as

$$\frac{\partial \overline{U_i}}{\partial t} = \overline{U_j}\frac{\partial \overline{U_i}}{\partial x_j} = -\frac{1}{\rho}\frac{\partial}{\partial x_j}\left[\overline{P}\delta_{ij} + \mu\left(\frac{\partial \overline{U_i}}{\partial x_j} + \frac{\partial \overline{U_j}}{\partial x_i}\right) - \rho\overline{u_i u_j}\right] \tag{2.16}$$

Eq (2.15) and (2.16) are the RANS (Reynolds Averaged Navier-Strokes) equations.

The $k - \epsilon$ model, based on RANS, is one of the most frequently used turbulence model in CFD simulations. The standard k-ϵ model is used here and the transport equations for k and ϵ are [10][9]:

$$\frac{\partial \rho k}{\partial t} + \mathrm{div}(\rho k\vec{U}) = \mathrm{div}[\frac{\mu_t}{\sigma_k}\mathrm{grad}k] + 2\mu_t S_{ij} \cdot S_{ij} - \rho\epsilon \tag{2.17}$$

$$\frac{\partial \rho\epsilon}{\partial t} + \mathrm{div}(\rho\epsilon\vec{U}) = \mathrm{div}[\frac{\mu_t}{\sigma_\epsilon}\mathrm{grad}k] + C_{1\epsilon}\frac{\epsilon}{k}2\mu_t S_{ij} \cdot S_{ij} - C_{2\epsilon}\rho\frac{\epsilon^2}{k} \tag{2.18}$$

where the eddy viscosity is

$$\mu_t = \rho C_u \frac{k^2}{\epsilon} \tag{2.19}$$

The Eq. (2.17), (2.18) and (2.19) have 5 adjustable constants as listed in Table 2.5.

Constant	C_μ	σ_k	σ_ϵ	$C_{1\epsilon}$	$C_{2\epsilon}$
Value	0.09	1.00	1.30	1.44	1.92

Table 2.5: Constants for the standard $k - \epsilon$ model

The standard wall function [10] is used to describe the near wall region.

2.2.4 Chemical-turbulence interaction model

Chemical reactions occur at the molecular level. The reacting molecules have to meet (a process governed by mixing) before they can react (a process governed by chemical kinetics). So it is great of importance to determine whether the mixing rate and/or the chemical kinetics is the limiting factor in the overall reaction rates in reactive turbulent flows.

The Dahmköhler number is a dimensionless number that describes the relative importance of mixing and kinetics in a turbulent reactive flow. It is defined as [8]:

$$Da = \frac{\text{Typical time required for mixing}}{\text{Typical time required for chemical reactions}} \tag{2.20}$$

If $Da \ll 1$, chemical kinetics are slow comparing to the mixing rate. If $Da \gg 1$, it is the other way around. But when $Da \approx 1$, the chemical kinetics and mixing rate are in the same order of magnitude.

If only chemical kinetics is of interest, reaction rates can be determined by Arrhenius kinetic expressions [11][12] as in Eq. (2.21) while turbulence mixing is ignored.

$$k = Ae^{-\frac{E_a}{RT}} \tag{2.21}$$

In Eq. (2.21), k [$\mathrm{mol} \cdot \mathrm{m}^{-3} \cdot \mathrm{s}^{-1}$] is the rate constant of a chemical reaction, T [K] is the temperature, A [K-mol-m^3] is the pre-exponential factor, E_a [J/mol] is the activation energy and R [$\mathrm{J} \cdot \mathrm{K}^{-1} \cdot \mathrm{mol}^{-1}$] is the universal gas constant. The approach is known as the Laminar Finite Reaction model, based on the work of Magnussen et al. [13], avoids calculating Arrhenius kinetics by assuming that the reactions are entirely controlled by turbulent mixing. In this model, the net production rate of species i due to reaction r is given by the smaller value of (2.22) and (2.23)

$$R_{i,r} = \nu^{'}_{i,r} M_{w,i} A \rho \frac{\epsilon}{k} \min_{R} \left(\frac{Y_R}{\nu^{'}_{R,r} M_{w,R}} \right) \tag{2.22}$$

$$R_{i,r} = \nu^{'}_{i,r} M_{w,i} A B \rho \frac{\epsilon}{k} \frac{\sum_P Y_P}{\sum_j^N \nu^{''}_{j,r} M_{w,j}} \tag{2.23}$$

where Y is the mass fraction, $A = 4.0$ and $B = 0.5$ are empirical constants, subscript P is any product species and R is a particular reactant.

In Ansys Fluent, the so called finite reaction/eddy-dissipation model uses the limiting factor (the mixing rate and/or the chemical kinetics) to determine the local, transient reaction rate.

2.2.5 Euler-Lagrange model and discrete random walk model

The Euler-Lagrange model is one of the most frequently used models for disperse multiphase flows when the particle volume loading is low so the effects of particles on the fluid and other particles can be treated with either one-way or two-way coupling. In the Euler-Language model, the fluid phase is treated as a continuum and can be modelled by using standard RANS models (for example, the standard $k - \epsilon$ model), and the effects of the dispersed phase (the droplets) are represented by source terms in the continuous phase balance equations. Each particle (or each bundle of particles) is tracked and its trajectory is calculated from Newton's second law of motion [8].

$$m_d \frac{\mathrm{d}U_{i,d}}{\mathrm{d}t} = F_{i,Drag} + F_{i,Press} + F_{i,Virt} + F_{i,History} + F_{i,Bouy} + F_{i,Lift} + F_{i,Therm} + F_{i,Turb} + F_{i,Brown} \tag{2.24}$$

where m_d is the particle mass, $U_{i,d}$ is the particle linear velocity, $F_{i,Darg}$ is the drag force, $F_{i,Press}$ is the pressure force due to pressure gradient, $F_{i,Virt}$ is the virtual mass force due to acceleration of surrounding fluid, $F_{i,History}$ is the history force due to changes in boundary layer, $F_{i,Lift}$ is the Saffman and Magnus lift force due to velocity gradient and particle rotation, $F_{i,Therm}$ is the thermophoretic force due to a temperature gradient, $F_{i,Turb}$ is the force due to turbulent fluctuations and $F_{i,Brown}$ is the Brownian force due to molecular collisions. In this thesis work, only $F_{i,Darg}$ and $F_{i,Bouy}$ are considered. Turbulent fluctuations are not modelled as a force, but as a variation of the continuous phase velocity seen by the droplets.

Since the dispersed phase is being tracked in a RANS flow field, a method must be used by which the particles are made to interact also with the turbulent fluctuations. In the work of Gosman et al. [14], an Eddy Interaction model is developed to describle particle dispersion in turbulent flow.

The Eddy Interaction model is a discrete random walk model that considers effects of the fluctuating flow field by making particles to interact with the instantaneous velocity. In this model, a particle is captured by an eddy with instantaneous velocity. Then the particle interact with another eddy after the lifetime of the previous eddy or the particle crosses the previous eddy. According to Gosman et al. [14], the length and lifetime of an eddy is

$$L_e = C_\mu^{\frac{3}{4}} \frac{k^{\frac{3}{2}}}{\epsilon} \tag{2.25}$$

$$\tau_e = C_L \frac{k}{\epsilon} \tag{2.26}$$

where $C_L = 0.3$ for $k - \epsilon$ model. The particle eddy crossing time is [15]

$$t_{cross} = -\tau \ln \left[1 - \left(\frac{L_e}{\tau \left| u - u_p \right|} \right) \right] \tag{2.27}$$

where τ is the particle relaxation time, L_e is the eddy time scale and $|u - u_p|$ is the magnitude of the relative velocity.

The velocity values of the fluctuating parts in their lifetimes are assumed to obey a Gaussian probability distribution [8],

$$u = \zeta_u \sqrt{\bar{u}^2} \tag{2.28}$$

$$v = \zeta_v \sqrt{\bar{v}^2} \tag{2.29}$$

$$w = \zeta_w \sqrt{\bar{w}^2} \tag{2.30}$$

where u, v, w are the fluctuating velocities in three directions and ζ means a normally distributed random number of zero mean and unit variance.

In the $k - \epsilon$ model, the fluctuating parts of fluid velocities are assumed to be isotropic and their root mean squared values are obtained via

$$\sqrt{\bar{u}^2} = \sqrt{\bar{v}^2} = \sqrt{\bar{w}^2} = \sqrt{\frac{2}{3}k} \tag{2.31}$$

3 Case specifications

In this chapter, the different simulation cases are specified. The 1) urea evaporation and decomposition, and 2) NOx reduction are studied separately then they are simulated together as a whole process.

3.1 Urea evaporation and decomposition

In this section, only the urea decomposition and breakdown process is of interest. CFD model is used.

The computational domain is a 1m diameter, 5m long cylinder pipe (Figure 3.1). The inlet is plane $Z = 5$ m and outlet is plain $Z = 0$ m. Urea-water mixtures (Table 3.1) are injected from the inlet center, $(0, 0, 5)$ and mixed with the flue gases from the inlet (Table 3.2). The gas composition in Table 3.2 is a representative of the flue gases from a typical biomass boiler. The velocity of a diameter (the line of intersection of Plane XZ and the inlet plane) at the inlet of the flue gases follows Figure 3.2 and it is symmetric of the inlet center.

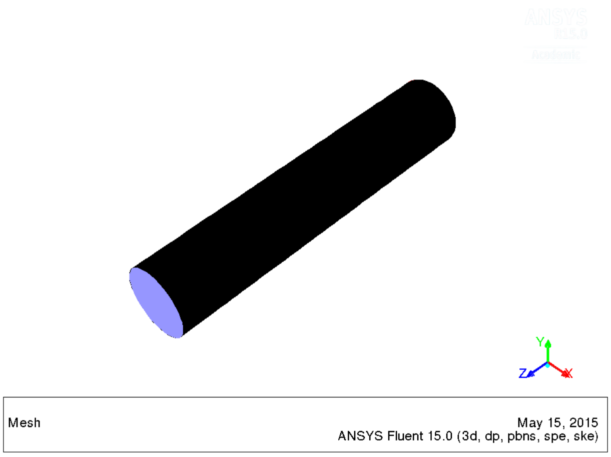

Figure 3.1: Geometry of the simple pipe

Parameter	Unit	Value
X position	m	0
Y position	m	0
Z position	m	4
X velocity	m/s	0
Y velocity	m/s	0
Z velocity	m/s	-25
Diameter	m	4.5E-5
Temperature	K	300
Flow rate	kg/s	0.002348578
Urea mass fraction		0.325
Water mass fraction		0.675

Table 3.1: Urea injection settings for urea decomposition and breakdown

In Case 1-4[1], particles are set to two different diameters (45 mm and 150 mm) in the simulation with/without discrete random walk model to investigate the effects of discrete random walk model as stated in Table 3.3. The inlet temperature is 1173 K for Case 1-4.

In Case 5-6, different chemical-turbulence interaction model is used to simulate only Reaction {2.2} to compare its mixing rate with chemical kinetics as stated in Table 3.4.

For Case 5-6, the inlet temperature is set to be 1223 K, the particle diameter is 45 μm and its injection velocity is -5 m/s in the Z-direction, the discrete random walk model is activated, other parameters are the

---

[1] The O_2 molar fraction at the inlet is 0.12 for Case 1-4.

Species	Molar fraction
NH_3	0
H_2O	0
HNCO	0
NO	0.00015
CO_2	0.062
O_2	0.04
$CO(NH_2)_2$	0
N_2	The rest

Table 3.2: Species molar fraction at the inlet for urea decomposition and breakdown

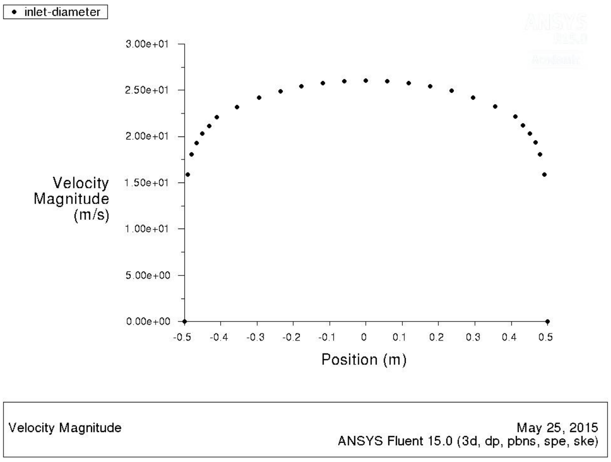

Figure 3.2: Inlet velocity

Case ID	Particle diameter [μm]	Discrete Random Walk Model
1	45	No
2	45	Yes
3	150	No
4	150	Yes

Table 3.3: Case 1-4

same as in Case 1-4.

Since Reaction {2.1} has only one reactant, if backward reaction is not considered, then the limiting factor of Reaction {2.1} is chemical kinetics, so there is no need to conduct similar simulations as Case 5-6.

Case ID	Chemical-turbulence interaction model
5	Laminar finite rate
6	Finite rate/Eddy-dissipation

Table 3.4: Case 5-6

3.2 NO_x reduction

In this section, only the NO_x reduction process is simulated with CSTR, PFR and CFD models with different settings by using premixed gases as inlet as in Table 3.5, the urea evaporation and decomposition processes are not included. In Case 7-13, the inlet is set to have flue gases with NH_3 premixed, instead of using urea spray injection to produce NH_3. Again, the data chosen in Table 3.5 is a representative of the flue gases from a typical biomass boiler.

The inlet temperature of the flue gases and its retention time influence the overall reaction rate. The simulation model decides how precise the results are and how computationally expensive the simulations are.

Species	Molar fraction
NH_3	0.00015
H_2O	0
HNCO	0
NO	0.00015
CO_2	0.062
O_2	0.04
$CO(NH_2)_2$	0
N_2	The rest

Table 3.5: Species molar fraction at the inlet for NO_x reduction

Based on the effects of inlet temperature and the simulation models, the cases in Table 3.6 are simulated with different inlet temperature and simulation models. By analyzing the data at difference positions, the effects of retention time can be investigated.

For Case 7-11, the discrete random walk model is activated and finite rate/eddy-dissipation is used as chemical-turbulence interaction model.

For Case 12-13[2], the inlet conditions are the same as in Case 8.

Case ID	Inlet temperature [K]	Simulation model
7	1173	CFD
8	1223	CFD
9	1273	CFD
10	1323	CFD
11	1373	CFD
12	1223	CSTR
13	1223	PFR

Table 3.6: Case 7-13

Similar to Case 5-6, Case 14-17 are set to determine the impacts of mixing and chemical kinetics of Reaction {2.3} and Reaction {2.4}.

However, in Case 14-17, Reaction {2.1} and {2.2} are included and the inlet and injection conditions are as the same as in Case 5-6. If the the premixed flue gases with NH_3 as inlet, the simulation results will not differ whether laminar finite rate model or finite rate/eddy-dissipation model is used as chemical-turbulence interaction model. In each case, only one reaction of Reaction {2.3} or {2.4} is simulated in the CFD model.

Case ID	Reaction	Chemical-turbulence interaction model
14	{2.1}, {2.2}, {2.3}	Laminar finite rate
15	{2.1}, {2.2}, {2.3}	Finite rate/Eddy-dissipation
16	{2.1}, {2.2}, {2.4}	Laminar finite rate model
17	{2.1}, {2.2}, {2.4}	Finite rate/Eddy-dissipation

Table 3.7: Case 5-6

3.3 Whole process

In this section, the whole process, meaning urea evaporation and decomposition and NO_x reduction all together, is simulated.

---

[2] 1223K is used based on the results that are shown in Figure 4.4: 1223K is the optimum temperature for NO_x reduction on the given conditions.

3.3.1 Simple pipe

In this part, the whole process is simulated in the CFD model. The inlet temperature is set to be 1223 K, the particle diameter is 45 μm and its injection velocity is -25 m/s in the Z-direction, the discrete random walk model is activated, finite rate/eddy-dissipation is used as chemical-turbulence interaction model, other parameters are the same as in Case 1-4.

Case ID	18
Temperature [K]	1223
Chemical-turbulence interaction model	Finite rate/Eddy-dissipation

Table 3.8: Case 18

3.3.2 Rörvik plant

In this section, a new geometry based on a real power plant Rörvik is used in the simulation as seen in Figure 3.3.

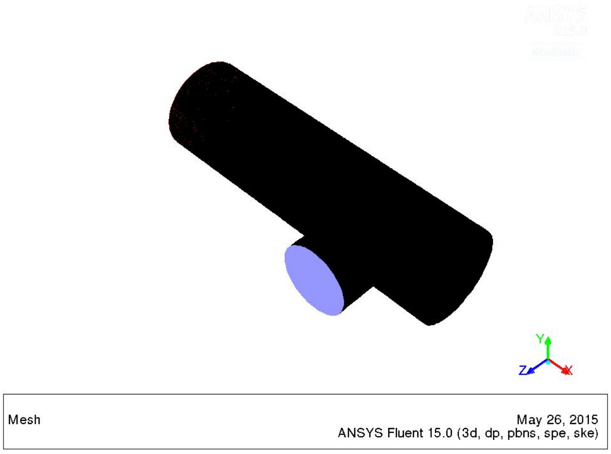

Figure 3.3: Geometry of the Rövik power plant urea SNCR system

The new geometry, as seen its sketch in Figure 3.4, can be considered as one small cylinder pipe ($DE = 0.57$ m, $EG = 1$ m) and one large cylinder ($AC = 1.35$ m) pipe connected together. The flues gases come from the inlet (Plane EG). The point where the central lines of the two pipes meet has the coordinate (0, 0, 0). The inlet is the plane where $Z = 1.245$ m, the outlet is the plane $X = -3.4$ m.

Firstly, a case based on the real operation environment (Case X) is simulated to validate the simulations as in Case 19. In Case 19, the injection conditions are listed in Table 3.9 which are typical values for commercial spray [16], the inlet conditions are listed in Table 3.10, finite rate/eddy-dissipation is used as the chemical-turbulence interaction model.

It is noted that when measuring data in Case X, the data is not collected at the inlet and outlet, but at the plane where $X = 0.2, -0.8, -1.8$ m, so assumptions have to be made for the inlet in the simulations.

Then based on Case 19, Case 20 with different injection plan is simulated. Comparing to Case 19, only the injection positions (Table 3.11) are changed in Case 20 to test the new injection point.

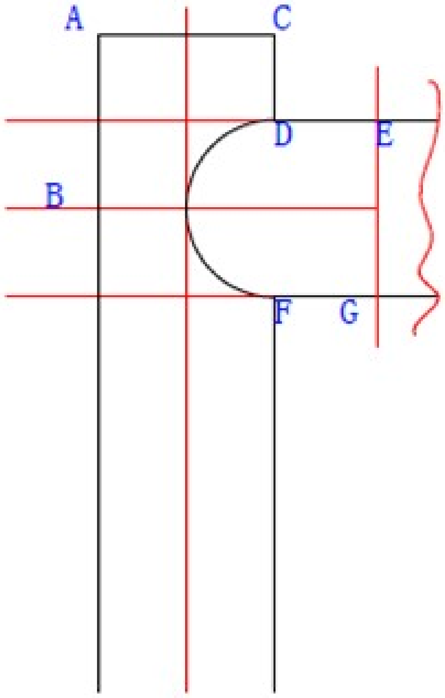

Figure 3.4: Sketch of Figure 3.3 in Y direction

Parameter	Unit	Value
X position	m	0.3
Y position	m	0
Z position	m	1.244
X velocity	m/s	-17.75
Y velocity	m/s	0
Z velocity	m/s	0
Diameter	m	0.0001
Temperature	K	300
Flow rate	kg/s	0.001240555
Urea mass fraction		0.3506
Water mass fraction		0.6494

Table 3.9: Urea injection settings for Rövik

Species	NH_3	H_2O	HNCO	NO	CO_2	O_2	$CO(NH_2)_2$	N_2
Molar fraction	2.325E-7	0.25	0	5.865E-5	0.0995	0.0228	0	The rest

Table 3.10: Inlet conditions for Rövik

Case ID	Injection positions [m]
19	(0.3, 0, 1.244)
20	(-0.5, 0, 0.475)

Table 3.11: Injection positions for Case 19-20

4 Results and discussions

Results based on the previous case specifications are presented and discussed in this chapter.

4.1 Effects of discrete random walk model on urea spray injection simulation

In the section, a brief summary of the results (that are based on Case 1-4) in Appended Paper A is presented.

From Figure 4.1 (Figure 2 in the paper), with discrete random walk model, the radial dispersion of droplets is obvious, comparing to the ones without discrete random walk model.

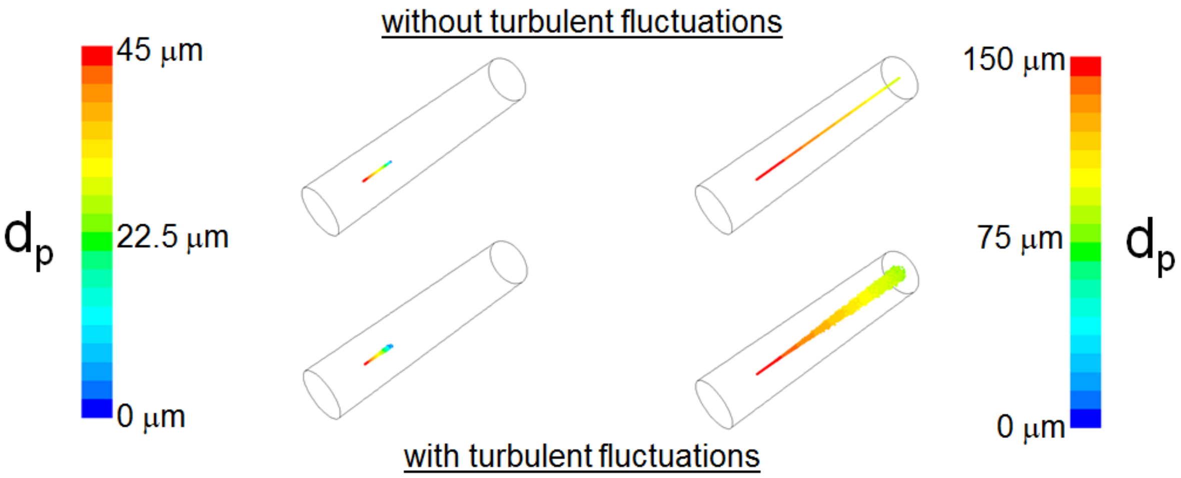

Figure 4.1: Illustrations of the predicted spray evolution for four computational urea-SNCR cases, the initial droplet size is either 45 (left) or 150 m (right) and the model for turbulent dispersion of the droplets is either turned on (bottom) or off (top)

As seen in Figure 4.2 and 4.3 (Figure 3 in the paper), the distribution of Reynolds number of the particles in the four compared cases are different. Larger Reynolds number comes with discrete random walk model, which means in cases that considers turbulent fluctuations, the larger relative velocities between the dispersed phase (droplets) and the continuous phase (gases) exist. With discrete random walk model, the temperature tends to distribute in a higher range. These observations indicate that a proper modeling of the effects of turbulent velocity fluctuations on the evaporation process is important for accurately describing the chemical kinetics, which are very sensitive to temperature.

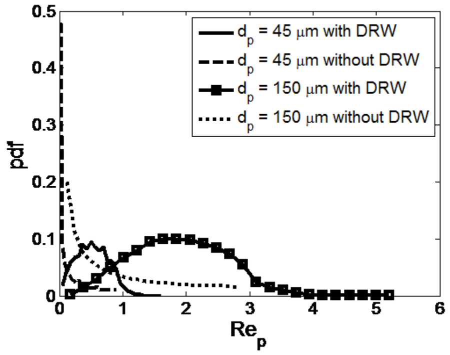

Figure 4.2: Probability distribution functions of droplet Reynolds number in the urea-SNCR simulations

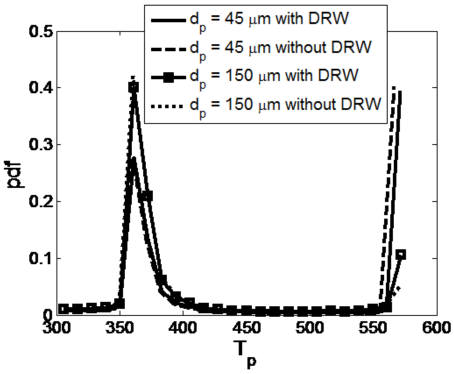

Figure 4.3: Probability distribution functions of droplet temperature in the urea-SNCR simulations

4.2 Effects of mixing and chemical kinetics on each reaction

In this section, effects of mixing and chemical kinetics on each reaction are investigated. Since the inlet temperature influences the chemical kinetics, different geometry and injection strategy lead to different mixing rate. It is therefore noted that these conclusions only strictly apply to this certain given condition, i.e. an inlet temperature of 1223 K, simple pipe as geometry, given injection strategy, etc.

As in Table 4.1 that are based on Case 5-6, NH_3 increases almost the same amount, so the limiting factor of Reaction {2.2}'s overall reaction rate is chemical kinetics or that the mixing rate and chemical kinetics have almost equal influences on the overall reaction rate.

Case ID	Chemical-turbulence interaction model	NH_3 inlet mass fraction	NH_3 outlet mass fraction
5	Laminar finite rate	0	4.14E-006
6	Finite rate/Eddy dissipation	0	4.14E-006

Table 4.1: NH_3 mass fraction of Case 5-6

As in Table 4.2 that are based on Case 14-15, NO reduction rate in Case 14 is higher than Case 15 (but not to a large extent), Reaction {2.3}'s overall reaction rate is more mixing controlled than chemical kinetics.

Case ID	14	15
Chemical-turbulence interaction model	Laminar finite rate	Finite rate/Eddy dissipation
NO inlet mass fraction	0.0001543264	0.0001543264
NO outlet mass fraction	0.0001228886	0.0001279279
NO reduction rate	20.37%	17.10%

Table 4.2: NH3 mass fraction of Case 14-15

As in Table 4.3 that are based on Case 16-17, only slightly more NO is produced in Case 16, the influences of mixing and chemical kinetics are almost in the same order for Reaction {2.4}.

Case ID	16	17
Chemical-turbulence interaction model	Laminar finite rate	Finite rate/Eddy dissipation
NO inlet mass fraction	0.0001543264	0.0001543264
NO outlet mass fraction	0.0001634442	0.0001631524
NO mass fraction increased by	5.91%	5.72%

Table 4.3: NH3 mass fraction of Case 16-17

4.3 Effects of temperature and retention time on NO_x reduction

In this section, the effects of temperature and retention time on NOx reduction are studied based on Case 7-11.

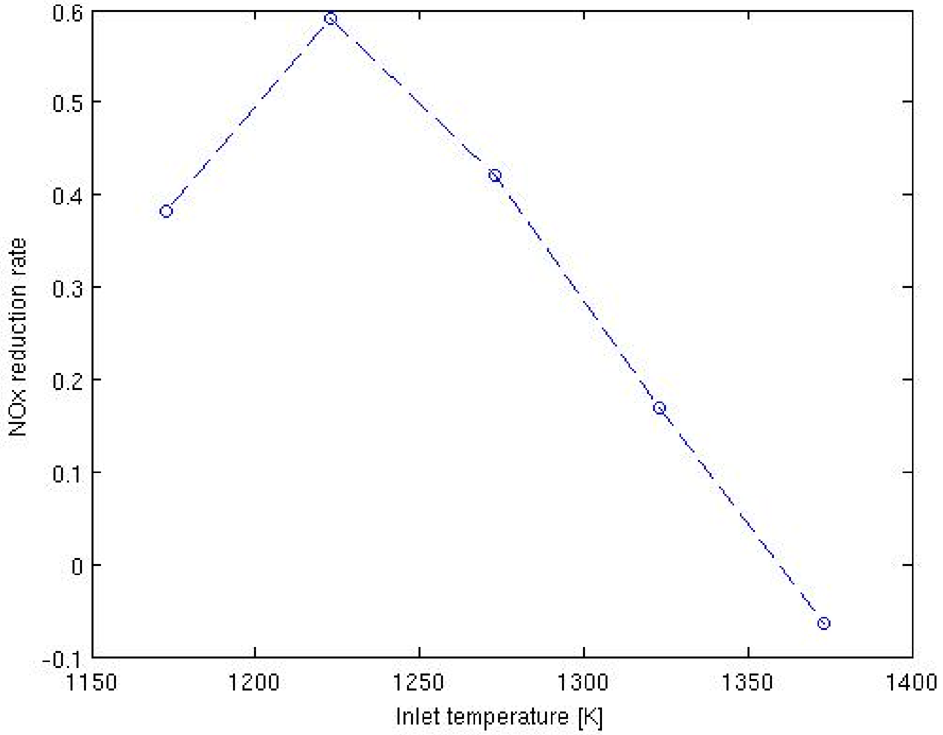

Figure 4.4: NO_x reduction rate to inlet temperature

As seen in Figure 4.4, as the temperature increases, the NO_x reduction rate increases to a peak, then decrease. It is also seen that the optimum temperature is around 1223 K. When the temperature is low, the chemical kinetics are not so fast, which causes the low reduction rate. When temperature increases, overall reaction rates of Reaction {2.3} and {2.4} both increases, but the increasing rates are different. Firstly, the Reaction {2.3} is dominant, so the NO_x reduction rate keeps increasing as the temperature increases, then Reaction {2.4}'s overall reaction rate increases faster than Reaction {2.3}, making the NO_x reduction rate decreases. If the temperature is high enough, Reaction {2.4} will be dominant, so more NO is produced, making the NO_x reduction rate negative.

For a given axial velocity, the distance from the inlet is directly proportional to the retention time. As shown in Figure 4.5, when the temperature is low, more retention time leads to better NO_x reduction results; when the temperature is high, the chemical reactions reach equilibrium very soon.

4.4 Model selection

Based on Case 8 (CFD model), Case 12 (CSTR model) and Case 13 (PFR model), Figure 4.6 is produced. In Case 13 (CFD model), the retention time is calculated by

$$\tau = l/v \tag{4.1}$$

where l [m] is the length and v [m/s] is the average inlet velocity.

It can be seen that the PFR model and the CFD model give similar results. Since in the CFD model, all the species have been perfectly premixed, so turbulence mixing cannot contribute or limit the simulation results, the overall reaction rates are calculated via Arrhenius kinetics gradually with retention time like in the PFR. Moreover, the PFR model here is based on a simple geometry (for example, a cylinder) which matches the geometry of CFD model used in Case 8, so the simulation mechanisms of PFR (Case 13) and CFD (Case 8) have a lot in common.

The CSTR model results are off comparing to the others. This is expected based on the assumptions of different models, where CSTR is a zero dimensional model in which it assumes the species concentrations are

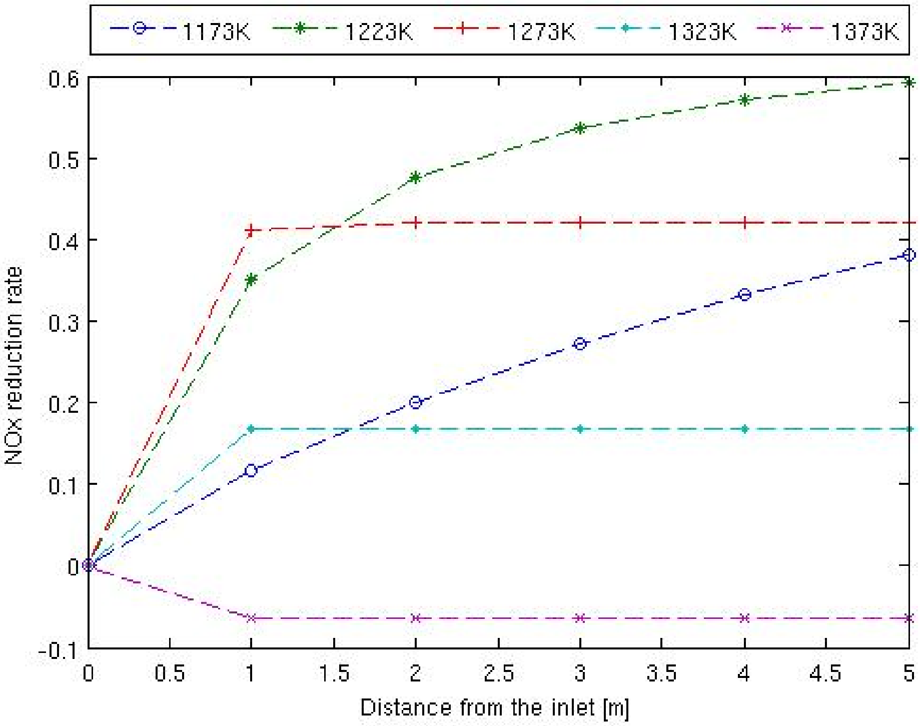

Figure 4.5: NO_x reduction rate at different positions and inlet temperatures

the same everywhere in the reaction tank, PFR is a one dimensional model which can be considered as a series of CSTR models, and the CFD model gives very detailed information in all the dimensions of the simulation domain. So the longer the pipe (retention time) is, the poorer the CSTR results are.

Therefore, CSTR model gives bad predictions and is not recommended[1], especially in a scenario with long retention time. For premixed inlet conditions without any injection in a simple geometry, a PFR model is sufficient. However, if the detailed field of a variable shall be obtained, use of a CFD model is advised.

4.5 CFD model validation

The simulation results of Case 19 are listed in Table 4.4 to be compared against the experimental data (Case X) to validate the CFD model.

Case ID	NO_x reduction rate
X	19.6%
19	15.8%

Table 4.4: NO_x reduction rate of Case X and Case 19

The NO_x reduction rate of Case 19 and X are off by as little as 3.8%, indicating that the CFD simulation can be still considered very applicable for the purpose of improving the injection strategy of industrial urea-SNCR processes.

The geometry used in Case 19 is a simplified geometry of the Rörvik (Case X) power plant urea-SNCR system. Moreover, as Case X was conducted for another project with another purpose, some data which are important for CFD simulations have not been collected. So in Case 19, several assumptions and simplifications are made (see Chapter 3.3.2). All these factors can contribute to the difference presented in Table 4.4.

---

[1] If the geometry where the reaction occurs is a recirculation zone, the CSTR model would be acceptable. However, this is a very unlikely reactor design for the urea-SNCR process.

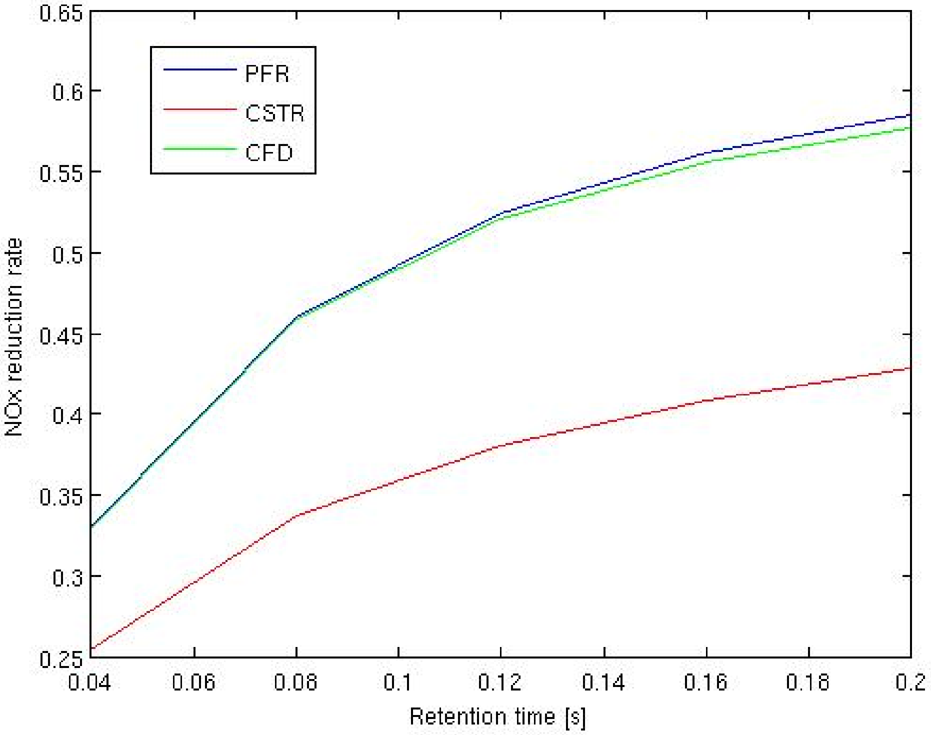

Figure 4.6: NO_x reduction rate at different retention times from Case 8, 12 and 13 at the inlet temperature 1223K

Case ID	19	X
$h = 1$ m	1144.86	1131.03
$h = 2$ m	1179.67	1180.42
$h = 3$ m	1179.31	1146.42

Table 4.5: Temperature [K] at different position in Case X and Case 19

As seen in Figure 4.7, there are three round cross-sectional planes, from the right to left, they are denoted as $h = 1$ m, $h = 2$ m and $h = 3$ m, representing the distance from Plane AC in Figure 3.4. In each cross-sectional plane, the temperature varies in a relatively large range. In the experiments (Case X), the data is collected at one point in each plane as in Table 4.5. If the data were collected somewhere else, or the data were collected in several different points in each cross-sectional planes, the data would be different. However, in the CFD simulations (Case 19), the temperature in Table 4.5 of each cross-sectional plane is calculated based of surface integrals of mass-averaged weight. The same philosophy also applies to NO measurement as seen in Figure 4.8. This also contributes the difference between Case 19 and X.

4.6 New injection test

A new injection point is tested in Case 20 instead the original one (Case 19) in the CFD simulations. As seen the results in Table 4.6, the NO_x reduction rate is lower. Since in Case 20, the new injection points are placed in the downflow compare to Case 19, it leads to less retention time, which explains such results.

Case ID	NO_x reduction rate
19	15.8%
20	5.5%

Table 4.6: NO_x reduction rate of Case 19 and 20

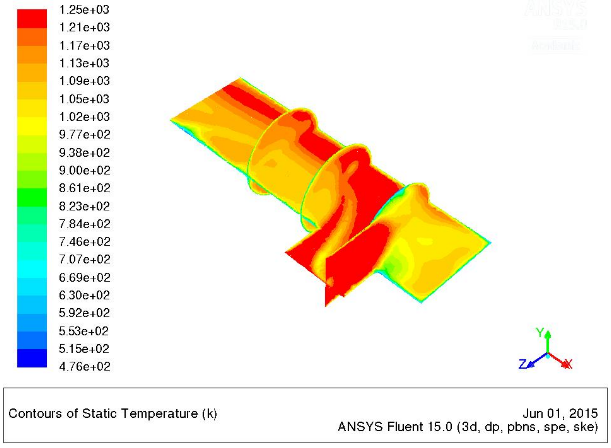

Figure 4.7: Temperature profile of Case 19

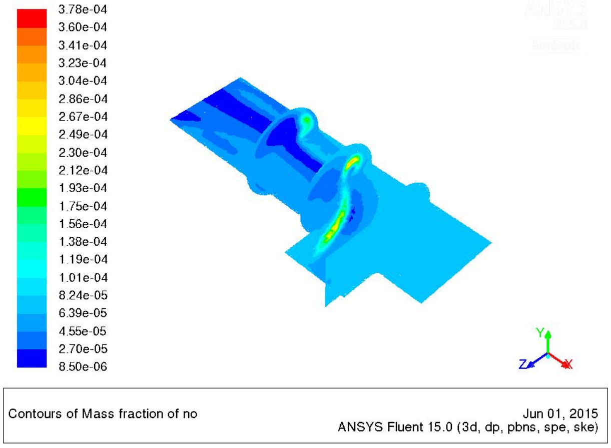

Figure 4.8: NO_x mass fraction profile of Case 19

5 Conclusions

An industrial urea-SNCR system has been investigated using reactor models and computational fluid dynamics (CFD). The following conclusions could be made:

1. Discrete random walk model affects the droplet dispersion and that it can influence the temperature at which the urea decomposes, which affects how CFD model simulates the urea spray.
2. In the given conditions, the limiting factors (mixing/chemical kinetics) for Reaction {2.2}, {2.3} and {2.4} have been studied. Reaction {2.2}'s overall reaction rate is more chemical kinetics controlled than mixing; Reaction {2.3} is the opposite; The influences of mixing and chemical kinetics are almost in the same order for Reaction {2.4}.
3. NO_x reduction has an optimum operating temperature around 1223 K for typical biomass flue gases in a simple geometry. At this temperature, the NO_x reduction rate increases as retention time increases.
4. The CSTR model yields poor predictions of the NO_x conversion, a PFR model gives similar predictions to a CFD model on the condition of perfect mixture inlet and simple geometry. For a real power plant with multiphase flow, CFD model is advised and validated against experiments. The NO_x conversion predicted in the CFD simulations agrees well with the available experimental measurements.
5. Based on the CFD simulation model, a new injection point is evaluated for the existing Rövik urea-SNCR system. The new injection point is however found to exhibit inferior performance compared to the original one.

6 Future work

In this chapter, several improvements for the continuation of this work are proposed.

Better chemical reaction mechanism can be used. For example, the two-step NO_x reduction process can be simulated based on the work of Farcy et al. [17].

Different CFD models can be tested (such as, using DES model instead $k - \epsilon$, change to different discrete random walk model) to see if it is worthwhile to use more complicated models to simulate the process.

It is also interesting to see investigate the turbulence mixing and chemical mechanism in detail at different temperatures. Similar model to discrete random walk model can be also deployed to account for the turbulent temperature and species concentrations fluctuations on the reaction rates.

When conducting experiment in the real power plant, data that are crucial to the simulation works should be collected, so the simulation models can be more comprehensively validated.

References

[1] A. Fritz and V. Pitchon. *The current state of research on automotive lean NOx catalysis.* 1997. DOI: `10.1016/S0926-3373(96)00102-6`.

[2] S. S. Sazhin. Advanced models of fuel droplet heating and evaporation. *Progress in Energy and Combustion Science* **32**.2 (Jan. 2006), 162–214. DOI: `10.1016/j.pecs.2005.11.001`.

[3] R. Miller, K. Harstad, and J. Bellan. Evaluation of equilibrium and non-equilibrium evaporation models for many-droplet gas-liquid flow simulations. *International Journal of Multiphase Flow* **24**.6 (Sept. 1998), 1025–1055. DOI: `10.1016/S0301-9322(98)00028-7`.

[4] A. Lundstrom et al. *Modelling of urea gas phase thermolysis and theoretical details on urea evaporation.* 2011.

[5] M. Østberg and K. Dam-Johansen. Empirical modeling of the selective non-catalytic reduction of no: comparison with large-scale experiments and detailed kinetic modeling. *Chemical Engineering Science* **49**.12 (June 1994), 1897–1904. DOI: `10.1016/0009-2509(94)80074-X`.

[6] R. Rota et al. Experimental and modeling analysis of the NOxOUT process. *Chemical Engineering Science* **57**.1 (Jan. 2002), 27–38. DOI: `10.1016/S0009-2509(01)00367-0`.

[7] G. W. Roberts. *Chemical reactions and chemical reactors.* John Wiley & Sons Hoboken, 2009.

[8] B. Andersson et al. *Computational Fluid Dynamics for Engineers.* 2011.

[9] H. K. Versteeg and W. Malalasekera. *An Introduction to Computational Fluid Dynamics: The Finite Volume Method.* 2007.

[10] B. Launder and D. Spalding. The numerical computation of turbulent flows. *Computer Methods in Applied Mechanics and Engineering* **3**.2 (Mar. 1974), 269–289. DOI: `10.1016/0045-7825(74)90029-2`.

[11] S. Arrhenius. Über die Dissociationswärme und den Einfluss der Temperatur auf den Dissociationsgrad der Elektrolyte (1889).

[12] S. Arrhenius. Über die Reaktionsgeschwindigkeit bei der Inversion von Rohrzucker durch Säuren. *Zeitschrift für physikalische Chemie* (1889).

[13] B. Magnussen and B. Hjertager. *On mathematical modeling of turbulent combustion with special emphasis on soot formation and combustion.* 1977.

[14] A. D. Gosman and E. Ioannides. *ASPECTS OF COMPUTER SIMULATION OF LIQUID-FUELED COMBUSTORS.* 1983.

[15] L. T. Choi et al. Flow and particle deposition patterns in a realistic human double bifurcation airway model. *Inhalation toxicology* **19**.2 (2007), 117–131.

[16] H. Ström, A. Lundström, and B. Andersson. Choice of urea-spray models in CFD simulations of urea-SCR systems. *Chemical Engineering Journal* **150**.1 (2009), 69–82.

[17] B. Farcy et al. Two approaches of chemistry downsizing for simulating selective non catalytic reduction DeNOx process. *Fuel* **118** (2014), 291–299.

List of Tables

2.1 Antoine constants for urea vapor pressure and temperature (406K-550K) 2
2.2 Saturation pressure [Pa] and temperature [K] of water vapor 2
2.3 Simplified chemical process of urea breakdown 3
2.4 Simplified chemical process of NOx reduction 3
2.5 Constants for the standard $k - \epsilon$ model 5
3.1 Urea injection settings for urea decomposition and breakdown 8
3.2 Species molar fraction at the inlet for urea decomposition and breakdown 9
3.3 Case 1-4 9
3.4 Case 5-6 9
3.5 Species molar fraction at the inlet for NO_x reduction 10
3.6 Case 7-13 10
3.7 Case 5-6 10
3.8 Case 18 11
3.9 Urea injection settings for Rövik 12
3.10 Inlet conditions for Rövik 12
3.11 Injection positions for Case 19-20 12
4.1 NH_3 mass fraction of Case 5-6 14
4.2 NH3 mass fraction of Case 14-15 14
4.3 NH3 mass fraction of Case 16-17 14
4.4 NO_x reduction rate of Case X and Case 19 16
4.5 Temperature [K] at different position in Case X and Case 19 17
4.6 NO_x reduction rate of Case 19 and 20 17

List of Figures

3.1 Geometry of the simple pipe 8

3.2 Inlet velocity 9

3.3 Geometry of the Rövik power plant urea SNCR system 11

3.4 Sketch of Figure 3.3 in Y direction 12

4.1 Illustrations of the predicted spray evolution for four computational urea-SNCR cases, the initial droplet size is either 45 (left) or 150 m (right) and the model for turbulent dispersion of the droplets is either turned on (bottom) or off (top) 13

4.2 Probability distribution functions of droplet Reynolds number in the urea-SNCR simulations . 13

4.3 Probability distribution functions of droplet temperature in the urea-SNCR simulations 14

4.4 NO_x reduction rate to inlet temperature 15

4.5 NO_x reduction rate at different positions and inlet temperatures 16

4.6 NO_x reduction rate at different retention times from Case 8, 12 and 13 at the inlet temperature 1223K 17

4.7 Temperature profile of Case 19 18

4.8 NO_x mass fraction profile of Case 19 18

Part I

Appended Paper A

Effect of Turbulent Velocity Fluctuations on the Convective Heat Transfer to Droplets Subjected to Evaporation and Thermolysis (Accepted by AIP Conference Proceedings)

The Effect of Turbulent Velocity Fluctuations on the Convective Heat Transfer to Droplets Subjected to Evaporation and Thermolysis

Ning Guo, Oskar Finnerman and Henrik Ström

Division of Fluid Dynamics, Department of Applied Mechanics
Chalmers University of Technology, SE-412 96 Gothenburg, Sweden

Abstract. The effect of turbulent velocity fluctuations on the convective heat transfer to single droplets in a turbulent channel flow are investigated numerically. It is found that for properties relevant to typical liquid spray applications, the convective heat transfer is enhanced with increasing droplet size and bulk Reynolds number. The combined effect of convective heat transfer enhancement and increased driving forces for heat and mass transfer due to droplet dispersion is thereafter investigated for a commercial spray application. The probability distribution functions of droplet properties in the spray are found to be significantly affected by the presence of turbulent velocity fluctuations in the carrier phase.

Keywords: turbulence, convective heat transfer, droplet flow.
PACS: 47.27.-i, 47.27.E-, 47.27.T-, 47.27.te, 47.55.D-, 47.70.Fw, 44.05.+e, 44.35.+c

INTRODUCTION

The evaporation of the droplets being sprayed into a turbulent gas flow is of considerable interest in a number of important industrial processes (e.g., combustion of liquids fuels, spray drying and gas-liquid mixing). One application of specific interest in the present work is that of a turbulent spray used as a means to deliver a reducing agent in liquid form to a turbulent exhaust gas. This process forms the basis for the selective catalytic and non-catalytic reduction of nitrogen oxides (NO_x) using urea (urea-SCR and urea-SNCR), which are common methods to regulate the emissions of NO_x from combustion processes onboard vehicles and in power plants. The primary aim is here to mix ammonia (NH_3) with the exhaust gases so that the NH_3 may react efficiently with the NO_x. Because of potential safety problems, a solution of urea in water is often preferred to pure NH_3, as urea anyhow forms the NH_3 needed when undergoing thermolysis. Consequently, the task of optimizing a urea-SCR or a urea-SNCR system often becomes a question of ensuring fast and efficient mixing and heating of the urea-water spray with the hot exhaust gases. For successful numerical optimization of the NO_x conversion efficiency of such a system, in-depth knowledge of the physics determining the relevant processes is therefore important.

There are several effects of turbulence on the evaporation of a droplet flow. The first effect stems from the fact that the turbulent velocity fluctuations of the carrier phase affect the convective heat transfer to the droplets. Similar effects arise from the turbulent temperature and species concentration fluctuations, which affect the driving forces for heat and mass transfer. A secondary effect from the turbulent velocity fluctuations is to disperse the droplets over a larger volume, which acts so as to increase the driving forces for heat and mass transfer to the bulk. Finally, at high droplet loadings, the turbulence characteristics of the continuous phase will be affected by the local presence of droplets.

NUMERICAL METHOD

The present work focuses on the effects of the turbulent velocity fluctuations of the carrier phase on the heat transfer to the droplets. The urea-SNCR process is thereafter used as a case study for an investigation of the combination of the effects of the velocity fluctuations and the droplet dispersion. The effects of turbulent velocity fluctuations on the predicted particle Nusselt numbers are investigated in a turbulent channel flow of varying bulk Reynolds number. The mean flow properties are taken from Kim et al. [1] and the fluctuating RMS properties are taken from Dreeben and Pope [2] (obtained at Re = 13,000). As the aim of this part of the work is to assess the magnitude of the influences of the turbulent velocity fluctuations, the Reynolds-number dependence of the fluctuating quantities is disregarded. This assumption is expected to lead to an underestimation of the streamwise fluctuations and a (smaller) overestimation of the wall-normal fluctuations, as shown by Wei and Willmarth [3]. The overall conclusion is thus that the use of RMS property correlations obtained at a fixed bulk Reynolds number will tend to produce conservative estimates.

For each bulk Reynolds number, the complete Nusselt number history is acquired for an ensemble of 10,000 particles over a time period equal to 100 times the particle response time. The particles are introduced at random locations over the duct cross-section at the local mean velocity of the gas and are assumed to rebound in inelastic collisions upon interaction with the wall. The particle position is updated from knowing its velocity, and the particle velocity is obtained from:

$$\frac{du_p}{dt} = \frac{18\mu}{\rho_p d_p^{\ 2}}\left(1 + 0.15 Re_p^{\ 0.687}\right)\left(\overline{u} + u' - u_p\right) \tag{1}$$

Here, u_p is the particle velocity, μ is the dynamic viscosity of the gas phase, ρ_p is the particle density, d_p is the particle diameter, Re_p is the particle Reynolds number, $\overline{u}$ is the gas phase mean velocity and u' is the current gas phase velocity fluctuation (both taken at the current location of the particle). The formulation used in equation (1) reflects the fact that the drag correlation of Schiller and Naumann is employed [4]. The time step used in the integration of these equations is two orders of magnitude smaller than the particle response time. The gas phase velocity fluctuation is updated according to an eddy-interaction model [5] as described by Dehbi [6]. The anisotropy of the velocity fluctuations in the near-wall region is correctly accounted for by the present method, and the random insertion of particles into the duct enables the acquisition of averaged data, representative for the complete system.

The Nusselt number correlation used to assess the turbulent effects on heat transfer is taken from Frössling [7]:

$$Nu = 2 + 0.552 Re_p^{\ 0.5}\,\mathrm{Pr}^{1/3} \tag{2}$$

In a case where turbulent velocity fluctuations are not accounted for, the inserted particles would simply follow the gas flow at zero relative velocity, resulting in a constant Nusselt number equal to 2. The Nusselt number history obtained for each particle is therefore compared to this value to determine the time-averaged increase in the Nusselt number.

The effects of turbulent velocity fluctuations, modeled via an eddy-interaction model, are also investigated in a commercial urea-SNCR process. The injection of the urea-water solution will result in two processes – evaporation of water and thermolysis of urea [8] – that are both heat-transfer limited and that can both be modeled as evaporation processes [9]. The non-isothermal, chemically reactive turbulent gas flow is modeled using the Standard k-ε turbulence model. The effects of velocity fluctuations on the droplet trajectories and heat transfer coefficients are accounted for via the Discrete Random Walk (DRW) model [6]. Two-way coupling is employed between the gas phase and the droplet phase, so that the secondary effect of the droplet dispersion (via the temperature and concentration fields) is accounted for as well. Turbulent fluctuations of the temperature and the species concentrations and turbulence modulation from the presence of droplets are neglected, however. It is to be expected that the effect of species concentration fluctuations is negligible, whereas the effect of temperature fluctuations, if included, would act so as to further increase the broadening of the particle diameter probability distribution function [10]. The injected droplets are assumed to follow a uniform diameter distribution of either 45 or 150 μm. The initial urea content is 32.5% by weight, the rest is water. The droplets are injected at 300K into exhaust of 1173K. The exhaust gases flow through a circular duct of 1 m diameter and 5 m length. The injector is located 1 m downstream the gas inlet and points in the co-current direction. The bulk Reynolds number is approximately 400,000.

RESULTS AND DISCUSSION

Typical time-histories of the particle Nusselt number in the turbulent channel flow are illustrated in Figure 1a for particles of two different diameters. The particles are inserted into the flow at the centerline between the two walls of the channel, and may thereafter move in the wall-normal direction (and hence in a direction of increasing or decreasing RMS fluctuation magnitudes and mean streamwise velocity) as dictated by equation (1). The smaller particle has a response time that is short in relation to the time scale of the turbulent fluctuations, and it can be seen how it interacts with only a few turbulent eddies during the investigated time span. Each time the smaller particle enters a new turbulent eddy, the relative velocity peaks, resulting in a peak also in the Nusselt number. Because of its short response time, the smaller particle is quickly accelerated by the eddy. The larger particle has more inertia and thus a longer response time, causing it to interact with a larger number of turbulent eddies during the investigated time span. The increased inertia also means that the particle will spend a significantly longer part of its life at a non-zero relative velocity to the carrier gas. It is clear from this figure that the average convective heat transfer coefficient to the droplet will be significantly affected by the turbulent velocity fluctuations.

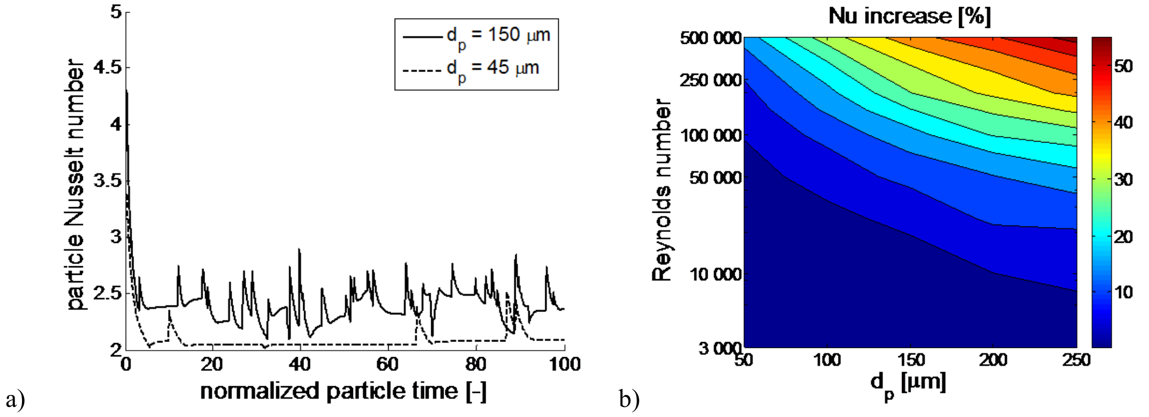

FIGURE 1. a) Illustration of the time-resolved fluctuations in the particle Nusselt number as a function of time (normalized by the particle response time). The bulk Reynolds number is 130,000.
b) Increase in the particle Nusselt number as a function of the bulk Reynolds number of the channel flow.

Figure 1b shows an overview of the effects of the turbulent velocity fluctuations on the average Nusselt number. The largest increase in the Nusselt number due to velocity fluctuations of the carrier phase are observed for large particles at high bulk Reynolds numbers. The increased effect at high Reynolds numbers is likely to be most significantly affected by the fluctuations in the wall-normal direction, as these fluctuations are the only ones moving the particles in a direction of changing mean velocity. Increasing the particle diameters implies increasing the particle response times, and hence explains why larger particles spend a comparatively longer time in relative motion to the fluid surrounding them. The observation by Berlemont et al. [10], that the effect is most pronounced for intermediate-sized droplets of approximately 100 μm diameter initially, is not valid here since the Lagrangian time scale of the turbulence of the fully developed channel flow is longer than that of the grid turbulence they used as a basis for their investigation.

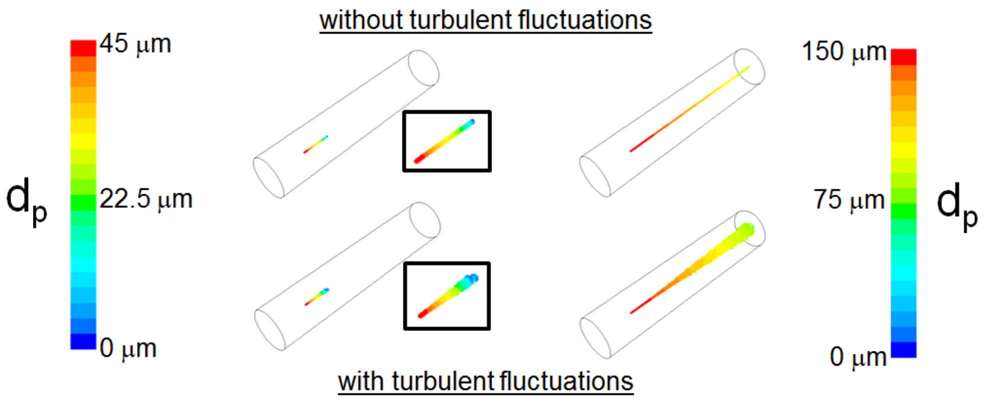

FIGURE 2. Illustrations of the predicted spray evolution for four computational urea-SNCR cases. The initial droplet size is either 45 (left) or 150 μm (right) and the model for turbulent dispersion of the droplets is either turned on (bottom) or off (top). The framed boxes show close-ups of the spray for the 45 μm cases.

Comprehensive numerical simulations accounting for the effects of varying mean temperature and species concentrations in the bulk as well as the diameter changes of the evaporating droplets are performed, and an overview of the results obtained from four such computational cases is shown in Figure 2. The radial dispersion of droplets that the turbulence is responsible for is clearly visible in this figure. It is also seen that the sizes of the droplets exiting the pipe in the case of 150 μm initial diameter is smaller than in the case where turbulent velocity fluctuations are not taken into account. A closer investigation of some of the droplet properties (particle Reynolds number and droplet temperature) is provided in Figure 3. The distribution of particle Reynolds numbers highlights the existence of larger relative velocities between the droplets and the gas in the cases where turbulent velocity fluctuations are accounted for. With the fluctuations accounted for, the distribution of droplet temperatures also shifts towards higher temperatures for the droplets undergoing thermolysis. The thermolysis temperature is determined by the balance of heat and mass transfer effects, and anything that has an effect on the convective heat transfer to the droplet will also affect the thermolysis process. As the urea that is produced then partakes in a set of fast and competing gas phase reactions, the thermolysis temperature is an important parameter for the overall prediction of the efficiency of a urea-SNCR system.

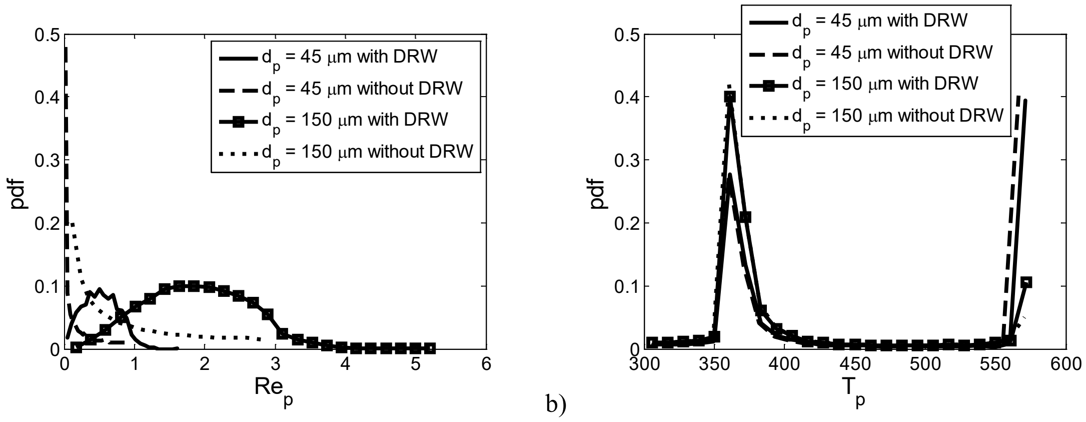

a) b)

FIGURE 3. Probability distribution functions of droplet properties in the urea-SNCR simulations: a) the droplet Reynolds number, and b) the droplet temperature.

CONCLUSIONS

In the current work, the enhancement of the convective heat transfer to droplets subjected to evaporation and/or thermolysis is investigated numerically. It is shown how the increase in the heat transfer coefficient, as predicted from an eddy-interaction model, increases with the droplet size and the Reynolds number of the bulk flow. Furthermore, the interplay of primary and secondary effects of turbulent velocity fluctuations on the heat transfer to a turbulent spray is investigated for a commercial urea-SNCR application. It is found that the predictions of the thermolysis temperature is sensitive to the modeling of turbulent velocity fluctuations.

REFERENCES

1. J. Kim, P. Moin and R. Moser, *J. Fluid Mech.* **177**, 133-166 (1987).
2. T. D. Dreeben and S. B. Pope, *Phys. Fluids* **9**, 154-163 (1997).
3. T. Wei and W. W. Willmarth, *J. Fluid Mech.* **204**, 57-95 (1989).
4. L. Schiller and Z. Naumann, *Zeitschrift des Vereines Deutscher Ingenieure* **77**, 318-320 (1935).
5. A. D. Gosman and E. Ioannides, *J. Energy* **7**, 482-490 (1983).
6. A. Dehbi, *Nucl. Eng. Des.* **238**, 707-715 (2008).
7. N. Frössling, *Gerl. Beitr. Zur Geophysik* **52**, 170-216 (1938).
8. H. Ström, A. Lundström and B. Andersson, *Chem. Eng. J.* **150**, 69-82 (2009).
9. A. Lundström, B. Waldheim, H. Ström and B. Westerberg, *J. Automobile Eng.* **225**, 1392-1398 (2011).
10. A. Berlemont, M.-S. Grancher and G. Gouesbet, *Int. J. Heat Mass Transfer* **34**, 2805-2812 (1991).